HONORS THESIS: EDGE DETECTION FROM INCOMPLETE AND NOISY FOURIER DATA

JESSICA JIANG*

Abstract. In applications such as magnetic resonance imaging (MRI) and synthetic aperture radar (SAR), the typically acquired Fourier measurements are noisy and under-sampled. Many methods have been developed to recover the underlying signal or its important structural information, such as its interior boundaries or edges. This thesis expands on the Fourier concentration method first introduced by Gelb and Tadmor in 1999. The modification is designed to increase adaptability of the concentration method so that it may be more generally employed in the context of computational inverse problems. In particular the resulting method can capture the behavior produced by sparsifying operators used in l^1 regularization techniques. Numerical experiments demonstrate that our new approach is accurate in recovering edge information of a one-dimensional signal and is also robust with respect to noise and undersampling.

1. Introduction.

In applications such as magnetic resonance imaging (MRI) and synthetic aperture radar (SAR), measurements are acquired as Fourier data, and are typically noisy and under-sampled. Filtering can help mitigate the effects of noise and reduce oscillatory artifacts but by design cause structure loss, since the solutions are "smoothed out". By contrast, iterative techniques such as l^1 regularization can encode structural information using sparse transform operators but are inherently more costly. If the edge information is known in advance, this encoding can be done more accurately and efficiently.

The concentration factor edge detection method is one technique used for locating these jumps [3]. These are Fourier space "filter" factors that "concentrate" the Fourier partial sum towards the singular support (or "edges") of the underlying function or image. Concentration factors have been specifically designed to handle more difficult edge recovery problems, such as when data has missing bands and large amounts of noise [3]. In this paper, we introduce a modification to the concentration factor design to include a regularization term. We would like our design to include an operator similar to that of the differencing operator in total variation, or TV regularization, because differencing operators are often used to recover edges from noisy data in the image domain. TV regularization also promotes the recovery of piecewise smooth solutions in computational inverse problems. However, with high levels of noise or missing bands of data in the Fourier domain, differencing operators, which can only be applied to physical space data, generally do not recover edges accurately. This motivates our new concentration factor design that will be able to better handle noisy and missing Fourier measurements. The rest of this thesis is organized as follows: In section 2 we review Fourier reconstruction of piecewise smooth functions [2] and the concentration factor method [3]. We introduce our new concentration factor designed to recover the differencing operator in section 3 and demonstrate its use in section 4. Some concluding remarks are provided in section 5.

2. Preliminaries.

Let f be a 2π-periodic piecewise smooth function defined in $[-\pi, \pi)$. The corresponding Fourier coefficients are defined as

$$\hat{f}_k = \frac{1}{2\pi} \int_{-\pi}^{\pi} f(x) e^{-ikx} dx. \tag{2.1}$$

*Department of Mathematics, Dartmouth College (jessica.l.jiang.25@dartmouth.edu)

Suppose we are given the first $2N+1$ noisy Fourier coefficients

$$\hat{f}^{\epsilon}_k = \hat{f}_k + \epsilon_k, \quad k = -N, \dots, N, \tag{2.2}$$

where $\{\epsilon_k\}_{k=-N}^{N} = \boldsymbol{\epsilon} \sim \mathcal{CN}(0, \sigma^2 I)$ is circularly symmetric and the variance σ^2 is obtained using the signal to noise ratio (SNR), which measures signal strength compared to noise level

$$n_k = \sqrt{\frac{P_{noise}}{2}}(\theta_k + i\omega_k).$$

Here θ_k and $\omega_k \sim \mathcal{N}(0, 1)$, and

$$P_{noise} = \frac{P_{signal}}{10^{\frac{SNR}{10}}}, \quad P_{signal} = \frac{||\hat{f}||_2^2}{2N+1}.$$

Observe higher SNR levels result in less noise, as the strength of the signal is more dominant.

The Fourier partial sum is defined as

$$S_N f(x) = \sum_{k=-N}^{N} \hat{f}_k e^{ikx}, \tag{2.3}$$

and for smooth and periodic functions $S_N f \to f$ exponentially [2]. Its discrete approximation on N_{grid} grid points is $\{S_N f(x_j)\}_{j=1}^{N_{grid}}$. However, when f is only piecewise smooth, (2.3) gives rise to the Gibbs phenomenon, which is characterized by the overshooting and undershooting oscillations around discontinuities. The overall order of accuracy is also reduced to $\mathcal{O}(\frac{1}{N})$ in smooth regions away from the discontinuities.

For instance, consider a square wave function defined as (recall $f(x+2\pi l) = f(x)$ for $l \in \mathcal{Z}$)

$$f(x) = \begin{cases} -1, & \text{if } -\frac{\pi}{6} + \frac{\pi}{3}m \le x < \frac{\pi}{6} + \frac{\pi}{3}m, \quad m = 0, \pm 2 \\ 1, & \text{otherwise} \end{cases} \tag{2.4}$$

Figure 1(left) displays the approximation of (2.4) using (2.3) and 129 Fourier coefficients. As expected, Gibbs oscillations can be seen at the interior jump discontinuity locations.

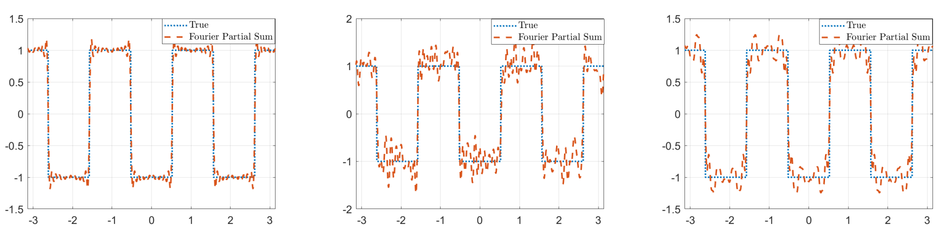

Figure 1: (left) Reconstruction of a square wave function using the standard Fourier partial sum; (middle) with SNR of 10; (right) missing Fourier bands of $-32 \le k \le -16 \cup 16 \le k \le 32$ and SNR of 10. Here $2N+1 = 129$.

The standard Fourier partial sum approximation is also quite sensitive to noise which can dominate the magnitude of the high frequency coefficients. Specifically, replacing $\hat{f}_k$ with $\hat{f}_k^\epsilon$ in (2.3) yields more undesirable oscillations, as seen in Figure 1(middle) where the SNR is 10. Finally, missing bands of Fourier data can also have unwanted effects that distort the reconstruction, as is evident in Figure 1(right) where the values of $\hat{f}_k$, $-32 \leq k \leq -16 \cup 16 \leq k \leq 32$, have been "zeroed out". Observe that the edges are less sharp and the correct amplitude at edge locations is hard to determine. The "missing band" case reflects the situation where the some data acquisitions might be unreliable.

While various techniques have been designed to improve the overall accuracy of the function approximation, in some applications it is important to simply know the locations of the jump discontinuities, for example in classification or identification algorithms. In other cases the signal recovery algorithm might benefit from first identifying such features in a pre-processing step. Hence we are motivated to design techniques that recover edges of piecewise smooth signals from their incomplete and noisy Fourier data.

2.1. The concentration factor edge detection method. We begin by describing the *concentration factor edge detection method*, which was introduced in [1] to determine the edges of a piecewise smooth periodic function $f(x)$ in $[-\pi, \pi)$ from its corresponding Fourier coefficients (2.1). This requires the following definition:

DEFINITION 1. *(Jump Function) Let the right and left-hand limits of the function, $f(x^+)$ and $f(x^-)$, be defined at every point x in the domain $[-\pi, \pi)$. The jump function associated with f and denoted by $[f]$ is defined as the difference between the right and left hand limits of the function at every point x; i.e.,*

$$[f](x) := f(x^+) - f(x^-). \tag{2.5}$$

Note that the jump function is non-zero only at a jump discontinuity, where it takes the value of the jump. We will use the terms "jump" and "edge" interchangeably throughout this exposition.

For ease of presentation, and without loss of generality, we consider that f only has a single discontinuity at the value $x = \zeta$. (Our numerical experiments contain multiple edges.) In this case we can also write (2.5) as

$$[f](x) = [f](\zeta) I_\zeta(x),$$

where $I_\zeta(x)$ is the indicator function with $I_\zeta(x) = 1$ when $x = \zeta$ and 0 otherwise. It follows from (2.1) that

$$\hat{f}_k = \frac{1}{2\pi}\int_{-\pi}^{\zeta^-} f(x)e^{ikx}dx + \frac{1}{2\pi}\int_{\zeta^+}^{\pi} f(x)e^{ikx}dx. \tag{2.6}$$

Using integration by parts, this becomes

$$\hat{f}_k = (f(\zeta^+) - f(\zeta^-))\frac{e^{-ik\zeta}}{2\pi ik} + \frac{1}{ik}(\frac{1}{2\pi}\int_{-\pi}^{\zeta^-} f'(x)e^{ikx}dx + \frac{1}{2\pi}\int_{\zeta^+}^{\pi} f'(x)e^{ikx}dx).$$

Continuing to integrate by parts, we obtain

$$\hat{f}_k = \frac{1}{2\pi}(\frac{[f](\zeta)}{ik} + \frac{[f'](\zeta)}{(ik)^2} + \frac{[f''](\zeta)}{(ik)^3} + \cdots \frac{[f^{(p)}](\zeta)}{(ik)^{p+1}} + \cdots)e^{-ik\zeta}, \quad k \neq 0,$$

where $[f^{(p)}](\zeta)$ denotes the jump discontinuity value of the pth derivative of f at ζ. It follows that

$$\hat{f}_k = [f](\zeta)\frac{1}{2\pi i k} + \mathcal{O}(\frac{1}{k^2}), \tag{2.7}$$

suggesting that one might be able to approximate $[f](\zeta)$ from the given Fourier coefficients $\{\hat{f}_k\}_{k=-N}^{N}$ in (2.1), and more generally $[f](x) = \sum_{j=1}^{J}[f](\zeta_j)I_{\zeta_j}(x)$ when $\{\zeta_j\}_{j=1}^{J}$ are distinct discontinuity locations of f on $[-\pi,\pi)$.

The concentration factor edge detection method, introduced in [1], locates the edges of a piecewise smooth function by "concentrating" its Fourier partial sum at the singular support. It is defined as:

$$S_N^\sigma[f](x) = i\sum_{k=-N,k\neq 0}^{N}\sigma(\frac{|k|}{N})\mathrm{sgn}(k)\hat{f}_k e^{ikx}. \tag{2.8}$$

The concentration factors $\sigma(\eta)$, $\eta \in (0,1)$, satisfy a set of admissibility conditions given by

1. $K_N^\sigma(x) = \sum_{k=1}^{N}\sigma(\frac{k}{N})\sin(kx)$ is odd;
2. $\frac{\sigma(\eta)}{\eta} \in \mathcal{C}^2(0,1)$;
3. $\int_\epsilon^1 \frac{\sigma(\eta)}{\eta} \to -\pi$, where $\epsilon = \epsilon(N) > 0$ is small.

Observe that $S_N^\sigma[f](x) = (K_N^\sigma * f)(x)$, meaning that convolving f with an odd function leads to "concentration" at its singular support. The second admissibility requirement enforces enough smoothness for convergence of (2.8), while the third ensures proper normalization. Some examples of concentration factors include

- Trigonometric: $\sigma_G(\eta) = \frac{\pi\sin(\pi\eta)}{\mathrm{Si}(\pi)}$, where $Si(\pi) = \int_0^\pi \frac{\sin(x)}{x}dx$.
- Polynomial: $\sigma_P^p(\eta) = p\pi\eta^p$. $p > 0$
- Exponential: $\sigma_E = \frac{\pi}{C}\eta e^{\frac{1}{\alpha\eta(\eta-1)}}$ where $C = \int_{\epsilon(N)}^{1-\epsilon(N)}\exp(\frac{1}{\alpha\tau(\tau-1)})d\tau$ and $\alpha > 0$.

Figure 2 plots each of these concentration factor for η discretized as $\frac{|k|}{N}$. Observe that the concentration factors behave like band pass filters which serve to enhance some of the high frequency information of the piecewise smooth function f.

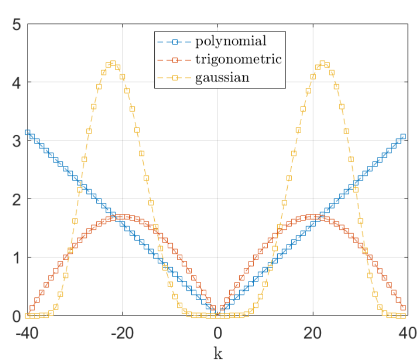

Figure 2: Plot of polynomial ($p = 1$), trigonometric, and Gaussian ($\alpha = 1$) concentration factors for $-40 \leq k \leq 40$.

If we seek to approximate $[f](x)$ on a set of N_{grid} equally spaced grid points, $x_j = -\pi + (j-1)\Delta x$, $j = 1, \dots, N_{grid}$ with $\Delta x = \frac{2\pi}{N_{grid}}$, we can write (2.8) in matrix vector notation. To this end, we define the inverse Fourier operator matrix $F_{inv} \in \mathbb{C}^{N_{grid} \times 2N+1}$ in terms of its components as

$$(F_{\text{inv}})_{jk} = e^{ikx_j}, \quad j = 1, \dots, N_{grid}, \quad k = -N, \dots, N,$$

which is appropriately shifted for computational purposes. Similarly, $\vec{\hat{f}} = \{\hat{f}_k\}_{k=-N}^{N} \in \mathbb{C}^{2N+1}$ is the vector of Fourier coefficients, $\vec{\sigma} = \{\sigma(|k|/N)\}_{k=-N}^{N} \in \mathbb{R}^{2N+1}$ corresponds to the vector of concentration factors evaluated at $|k|/N$, and $\vec{s} = \{1 \cdot \text{sgn}(k)\}_{k=-N}^{N} \in \mathbb{R}^{2N+1}$, then

$$\{S_N^\sigma[f](x_j)\}_{j=1}^{N_{grid}} = iF_{inv}(\vec{\hat{f}} \odot \vec{\sigma} \odot \vec{s}) \approx \{[f](x_j)\}_{j=1}^{N_{grid}}, \tag{2.9}$$

where $\odot$ represents componentwise multiplication. Note that due to cancellations and symmetries, (2.9) recovers real values.

2.2. Designing concentration factors. This investigation extends the concentration factor design method in [3] to consider other design properties, namely to be able to recover the first order finite difference of the discretized function $f(x_j)$, $j = 1, \dots, N_{grid}$, which will be described more in detail in section 3. For self containment purposes, the basic methodology for concentration factor design is reviewed below. More details can be found in [3]. We note that in contrast to the original concentration factor method based on admissible concentration factor *functions*, $\sigma(\eta)$, the concentration factor design method, seeks a concentration factor *vector* $\vec{\sigma}$ such that (2.9) is satisfied for x_j, $j = 1, \dots, N_{grid}$.

We begin by defining the unit ramp function $r(x)$ as

$$r(x) = \begin{cases} \frac{-\pi - x}{2\pi} & x < 0 \\ \frac{\pi - x}{2\pi} & x \geq 0. \end{cases} \tag{2.10}$$

The corresponding jump function is

$$[r](x) = \begin{cases} 1 & x = 0 \\ 0 & else. \end{cases} \tag{2.11}$$

The Fourier coefficients (2.1) of $r(x)$ are easily determined as

$$\hat{r}_k = \begin{cases} \frac{1}{2\pi ik}, & k \neq 0, \\ 0, & k = 0. \end{cases} \tag{2.12}$$

When comparing (2.12) to (2.7), it is evident that

$$\hat{f}_k \approx [f](0)\hat{r}_k,$$

that is, a low order approximation to the unknown quantity $[f](0)$ (in this case, by definition of the ramp function, the discontinuity occurs at $\zeta = 0$) can be obtained by modeling the known $\hat{f}_k$ in terms of the the ramp function coefficients. Based on the linearity of the Fourier partial sum (2.3) it follows that

$$[f](x) \approx [f](0)r(x). \tag{2.13}$$

A few remarks are in order.

Remark 2.1. [Translation of discontinuity.] We could also define the ramp function to have the discontinuity at $x = \zeta$. In this case we write $r_\zeta(x) = r(x-\zeta)$, with $\widehat{r_\zeta}_k$ appropriately translated in (2.1). The relationship between (2.12) and (2.7) still holds with $\hat{f}_k \approx [f](\zeta)\widehat{r_\zeta}_k$.

Remark 2.2. [Superposition of ramp functions.] It then follows that a piecewise smooth periodic function has a linear approximation which we can write as

$$f(x) \approx \sum_{j=1}^{J} \alpha_j r_{\zeta_j}(x),$$

for some coefficients α_j, $j = 1, \dots, J$. For the purposes of edge detection, this linear approximation to $f(x)$ is sufficient, since we are not interested in recovering the variability in the smooth regions.

To design the concentration factors, we first note that W.L.O.G, for a periodic function in $[-\pi, \pi)$ with a singular jump at $x = \zeta$, it follows from (2.1) that (2.9) can be written as

$$\begin{aligned}
S_N^\sigma[f](x) &= \sum_{0<|k|\le N} \hat{f}_k\, i\, \sigma\left(\frac{|k|}{N}\right)\operatorname{sgn}(k)e^{ikx} \\
&= \sum_{0<|k|\le N} \left[\frac{1}{2\pi}\left(\frac{[f](\zeta)}{ik} + \frac{[f]'(\zeta)}{(ik)^2} + \cdots\right)e^{-ik\zeta}\right] i\, \sigma\left(\frac{|k|}{N}\right)\operatorname{sgn}(k)e^{ikx} \\
&= \frac{[f](\zeta)}{2\pi}\sum_{0<|k|\le N} \frac{\sigma\left(\frac{|k|}{N}\right)\operatorname{sgn}(k)}{k} e^{ik(x-\zeta)} \\
&+ \frac{[f'](\zeta)}{2\pi}\sum_{0<|k|\le N} \frac{\sigma\left(\frac{|k|}{N}\right)\operatorname{sgn}(k)}{ik^2} e^{ik(x-\zeta)} \\
&+ \frac{[f''](\zeta)}{2\pi}\sum_{0<|k|\le N} \frac{\sigma\left(\frac{|k|}{N}\right)\operatorname{sgn}(k)}{i^2k^3} e^{ik(x-\zeta)} + \cdots
\end{aligned} \tag{2.14}$$

Based on (2.13) and the surrounding discussion, we write the first term on the right hand side of (2.14) as $[f](\zeta)W_0^{\sigma,N}(x-\zeta)$, where the signature profile $W_0^{\sigma,N}(x)$ is defined as

$$W_0^{\sigma,N}(x) := S_N^\sigma[r](x) = i\sum_{k=-N,k\ne 0}^{N} \sigma(\frac{|k|}{N})\operatorname{sgn}(k)\hat{r}_k e^{ikx_j} = \frac{1}{2\pi}\sum_{k=-N,k\ne 0}^{N} \frac{\sigma(\frac{|k|}{N})}{|k|}\hat{r}_k e^{ikx_j} \tag{2.15}$$

with $\hat{r}_k$ defined in (2.12). The remaining terms in (2.14) describe higher order jump responses, which we write as

$$W_1^{\sigma,N}(x) = \sum_{0<|k|\le N} \frac{\sigma\left(\frac{|k|}{N}\right)\operatorname{sgn}(k)}{2\pi i k^2} e^{ikx}, \quad W_2^{\sigma,N}(x) = \sum_{0<|k|\le N} \frac{\sigma\left(\frac{|k|}{N}\right)\operatorname{sgn}(k)}{2\pi i^2 k^3} e^{ikx},$$

and more generally

$$W_q^{\sigma,N}(x) = \sum_{0<|k|\leq N} \frac{\sigma\left(\frac{|k|}{N}\right)\operatorname{sgn}(k)}{2\pi i^q k^{q+1}} e^{ikx}.$$

Substituting the jump responses back into (2.14) yields

$$\begin{aligned} S_N^\sigma[f](x) &= [f](\zeta)W_0^{\sigma,N}(x-\zeta) + [f'](\zeta)W_1^{\sigma,N}(x-\zeta) + [f''](\zeta)W_2^{\sigma,N}(x-\zeta) + \cdots \\ &= [f](\zeta)W_0^{\sigma,N}(x-\zeta) + \mathcal{O}\left(\frac{1}{N}\right). \end{aligned} \tag{2.16}$$

As already noted, without loss of generality we can translate (2.16) so that the discontinuity occurs at $x = 0$, yielding $S_N^\sigma[f](x) \approx [f](0)W_0^{\sigma,N}(x)$. It follows that $\vec{\sigma}$ should be constructed so that its components $\sigma_k = \sigma(\frac{|k|}{N})$ generate the corresponding $W_0^{\sigma,N}(x)$ to behave like the indicator function, given by

$$\delta_0(x) = \begin{cases} 1 & x = 0 \\ 0 & else \end{cases} \tag{2.17}$$

in order to best approximate $[f](x)$. Once again we note that $\delta_0(x)$ can be translated to accommodate the discontinuity at $x = \zeta$, which would inevitably lead to the same design. The concentration factor design method seeks to satisfy $W_0^{\sigma,N}(x_j) = \delta_0(x_j)$, $j = 1, \ldots, N_{grid}$ which leads to the minimization problem:

$$\begin{aligned} &\min_\sigma ||W_0^{\sigma,N}||_2 \\ &\text{subject to } W_0^{\sigma,N}|_{x=0} = 1. \end{aligned}$$

Other constraints can be used to ensure the appropriate choice of $\vec{\sigma}$, including

- The components of $\vec{\sigma}$ are all non-negative, with $\sigma(1) = 0$ and $\sigma(N) = 0$. This leads to:

$$\begin{aligned} &\min_\sigma ||W_0^{\sigma,N}||_2 \\ &\text{subject to} \quad W_0^{\sigma,N}\Big|_{x=0} = 1 \\ &\qquad\qquad\quad \sigma_k \geq 0 \\ &\qquad\qquad\quad \sigma_1 = \sigma_N = 0 \end{aligned}$$

- In addition to the above constraints, we also seek to restrict the jump response to be small beyond the immediate area around the jump locations (reduction of oscillatory responses):

$$\begin{aligned} &\min_\sigma ||W_0^{\sigma,N}||_2 \\ &\text{subject to} \quad W_0^{\sigma,N}\Big|_{x=0} = 1 \\ &\qquad\qquad\quad \sigma_k \geq 0 \\ &\qquad\qquad\quad \sigma_1 = \sigma_N = 0 \\ &\qquad\qquad\quad \Big|W_0^{\sigma,N}\Big|_{|x|\geq\epsilon} \leq tol. \end{aligned}$$

- Finally, we address the case where some bands of Fourier data might be missing. That is, we define $k_{missing}$ as the range of integers $k \in [k_{min}, k_{max}] \cup$ $k \in [-k_{max}, -k_{min}]$ for which $\hat{f}_k$ is unknown. In this case we desire $\sigma(k) = 0$ for $k \in k_{missing}$, yielding the optimization problem

$$
\begin{aligned}
&\min_{\sigma} ||W_0^{\sigma,N}||_2 \\
&\text{subject to} \quad W_0^{\sigma,N}\Big|_{x=0} = 1 \\
&\qquad\qquad\qquad \sigma_k \geq 0 \\
&\qquad\qquad\qquad \sigma_k = 0, \quad k \in k_{missing} \\
&\qquad\qquad\qquad \sigma_1 = \sigma_N = 0 \\
&\qquad\qquad\qquad \left|W_0^{\sigma,N}\right|_{|x|\geq\epsilon} \leq tol.
\end{aligned}
$$

In our examples, we use $\epsilon = .35$ and $tol = 10^{-2}$. In general these values depend on N and $k_{missing}$.

Remark 2.3 (Discrete versus continuous approximation). It is important to note that the original concentration factor edge detection method is an approximation to the jump function, and that admissible concentration factors are functions defined on $[0, 1]$. The concentration factor design method solves the minimization problem for the discrete vector $\vec{\sigma}$ for the recovery of the jump function at a given set of grid point values. To avoid cumbersome notation we still write σ and x in the description of the design problem and only make a distinction using vector notation when needed.

3. Concentration Factor Modified Design. The main purpose of this investigation is to expand on the concentration factor design previously discussed to further include the ability to estimate the predicted edges of $L\vec{f}$ using different operators L, such as finite differencing operators of various orders. As already noted, first order differencing is often used as an edge detector for functions with sparse gradients in the physical domain. We define the first order differencing matrix $L_1 \in \mathbb{R}^{N_{grid}-1\times N_{grid}}$ as

$$
L_1 = \begin{bmatrix} -1 & 1 & 0 & 0 & \cdots & 0 \\ 0 & -1 & 1 & 0 & \cdots & 0 \\ 0 & 0 & -1 & 1 & \cdots & 0 \\ \vdots & \vdots & \vdots & \vdots & \ddots & \vdots \\ 0 & 0 & 0 & 0 & \cdots & 1 \end{bmatrix}.
$$

Figure 3 shows the application of L_1 on the square wave function defined in (2.4). Observe that $L_1\vec{f}$ recovers the the edge locations at specific grid point locations x_j, $j = 1, \ldots, N_{grid}$.

However, using the Fourier partial sum (2.3) with noisy Fourier coefficients $\hat{f}_k^{\epsilon}$ and missing bands of data to approximate $\vec{f}$ yields inaccurate results when doing first order differencing. Results in Figure 4 demonstrate that neither $LF_{inv}\vec{\hat{f}}_{band}$ nor $LF_{inv}\vec{\hat{f}}^{\epsilon}_{band}$ accurately recover the jump amplitudes, meaning that we need to seek other methods for edge recovery when handling noisy and missing data.

To design the concentration factors that can recover the edges for $L\vec{f}$, we first need to transform $L\vec{f}$ to the Fourier domain. This is accomplished using the discrete

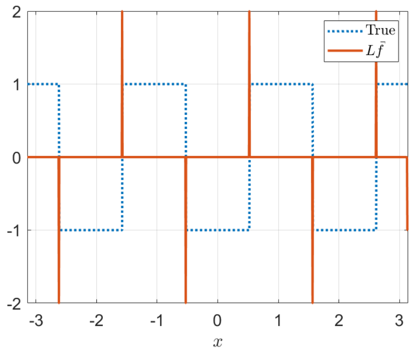

Figure 3: Plot of a square wave function with edges found through first order finite differencing matrix L_1.

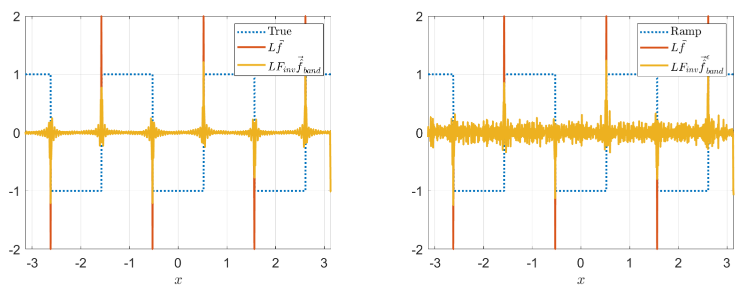

Figure 4: Plot of a square wave function with edges found through first order finite differencing using $LF_{inv}\vec{\hat{f}}$ as an approximation of $L\vec{f}$. We use 1025 Fourier coefficients and missing bands of $-256 \leq k \leq -128 \cup 128 \leq k \leq 256$. (left) no additional noise; (right) SNR is 20dB. The new designed concentration factor results are also shown for each case (red).

Fourier transform operator, with components defined as

$$F(k, j) = \frac{1}{N_{grid}} e^{-ikx_j}, \quad -N \leq k \leq N, \quad j = 1, \ldots, N_{grid} \tag{3.1}$$

for equally spaced grid points $x_j = -\pi + (j-1)\frac{2\pi}{N_{grid}}$. The idea is then that $(FL\vec{f})_k \approx i\hat{f}_k\sigma_k \text{sgn}(k)$ in (2.8). As before, we also exploit the relationship in (2.13) and use $\vec{r}$ for our design purposes. Finally, we use the "missing band" discrete Fourier transform matrix

$$(F_{mb})(k, j) = \begin{cases} 0 & \text{if } k \in k_{missing} \\ F(k, j) & \text{otherwise} \end{cases} \tag{3.2}$$

so that we do not try to use information that is unavailable to us to construct $\vec{\sigma}$. This leads us to the "baseline" design problem,

$$\begin{aligned} &\min_{\vec{\sigma}} \quad \left\| i\vec{\hat{f}} \odot \vec{\sigma} \odot \vec{s} - F_{mb} L \vec{r} \right\|_2 + \lambda \left\| W_0^{\sigma,N} \right\|_2 \\ &\text{subject to} \quad W_0^{\sigma,N}\big|_{x=0} = 1 \end{aligned}$$

where we have defined the components of $\vec{s}$ as $s_k = sgn(k)$ and $\odot$ again means componentwise multiplication. The regularization term $\left\| W_0^{\sigma,N} \right\|_2$ is included for robustness, with parameter λ chosen to minimize the impact of missing bands of information.

Following the constraint considerations described above, we write the general minimization problem as

$$\begin{aligned} \min_{\vec{\sigma}} \quad & \left(||i\vec{\hat{f}} \odot \vec{\sigma} \odot \vec{s} - F_{mb} L \vec{r}||_2 + \lambda ||W_0^{\sigma,N}||_2 \right) \\ & \text{subject to} \quad W_0^{\sigma,N}\big|_{x=0} = 1 \\ & \sigma_k \geq 0 \\ & \sigma_1 = \sigma_N = 0 \\ & \sigma_k = 0, \quad k \in k_{missing} \\ & \left| W_0^{\sigma,N} \right|_{|x| \geq \epsilon} \leq tol. \end{aligned} \tag{3.3}$$

As before, in our examples we choose $\epsilon = .35$ and $tol = 10^{-2}$. In general these values depend on N and $k_{missing}$.

4. Numerical Experiments. We now test our method on various test functions with different amounts of Fourier data (N), noise (SNR), and missing bands of information ($k_{missing}$).

Ramp Function. We first test the operator $L = L_1$, or the first order finite differencing operator. We use the ramp function $r(x)$ defined in (2.10) as our first test function. Since $r(x)$ is also used to design $\vec{\sigma}$, we anticipate good recovery of the edges of $L\vec{f} = L\vec{r}$. Figure 5 compares the results of using (2.9) with the approximation of $L\vec{f}$ (which would not be available) and $LF_{inv}\vec{\hat{f}}$ with $N = 1025$. We also show the designed concentration factors $\vec{\sigma}$. It is evident that $LF_{inv}\vec{\hat{f}}$ does not yield the correct jump location and amplitude of 1 at $x = 0$. To complicate the problem, we then add varying levels of noise by changing the SNR, with results using SNR = 10, 20, and 100 shown in Figure 6.

Even with SNR = 10, the highest noise level, it is clear that the jump function still maintains the correct amplitude and jump location. This is promising as many real-world problems have high levels of noise.

Next, we test the use of our designed concentration factors with missing bands of data. We impose missing bands of $-256 \leq k \leq -128 \cup 128 \leq k \leq 256$ for 1025 Fourier coefficients and show the result of the jump function reconstruction and the designed concentration factors in fig. 7

The concentration factors, as can be seen in panel b) of fig. 7, are zeroed out for the area of the missing bands on both the positive and negative side. The reconstruction of the jump function, however, remains intact with the correct jump height and location.

Lastly, we compare the use of our new designed concentration factors with other standard concentration factors as mentioned in sec. 2.2. We first look at the noiseless

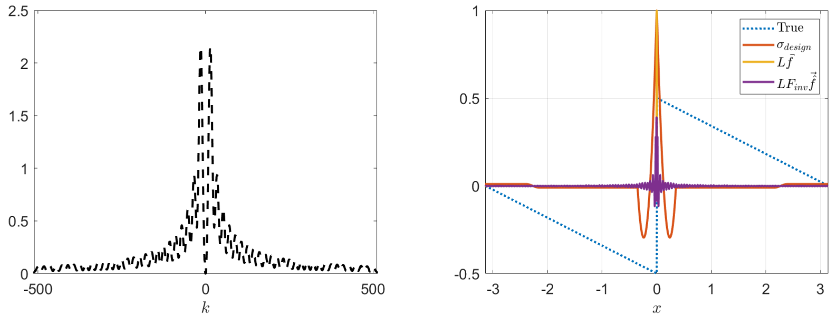

Figure 5: Ramp function in noiseless case with no missing bands. (left) Concentration vector $\vec{\sigma}$ found in (3.3); (right) Edge approximation (2.9) using designed concentration factors (red) compared to $L_1 F_{inv}\vec{\hat{f}}$ (purple) and the true finite difference edge recovery $L\vec{f}$ (yellow).

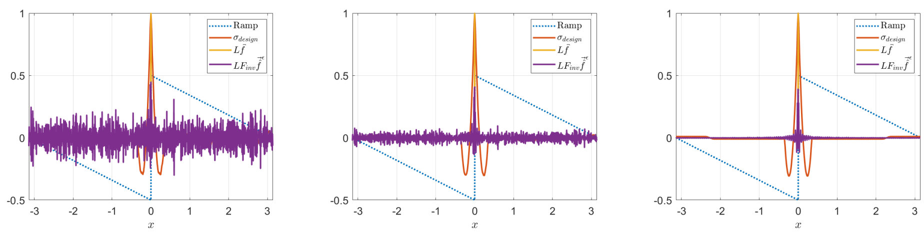

Figure 6: Jump function using designed concentration factors for the ramp function with SNR = (left) 10; (middle) 20; and (right) 100 dB.

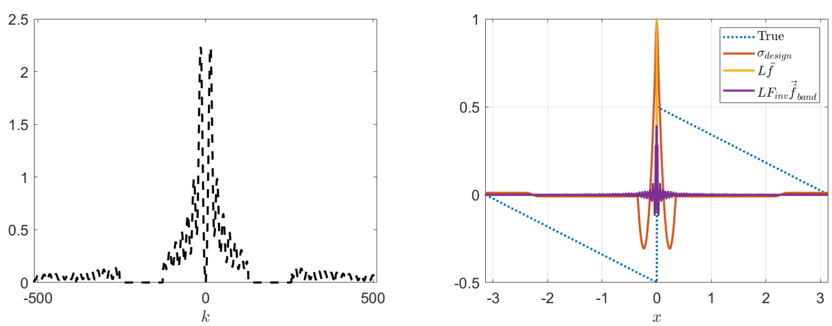

Figure 7: Ramp function in noiseless case with missing bands $-256 \leq k \leq -128 \cup 128 \leq k \leq 256$. (left) Concentration vector $\vec{\sigma}$ found in (3.3); (right) Edge approximation (2.9) using designed concentration factors (red) compared to $L_1 F_{inv}\vec{\hat{f}}_{band}$, where $\vec{\hat{f}}_{band}$ is the vector of Fourier coefficients accounting for missing bands (yellow).

case with no missing data in fig. 8. We note that we zero out any concentration factors in the Gaussian case where we divide by 0.

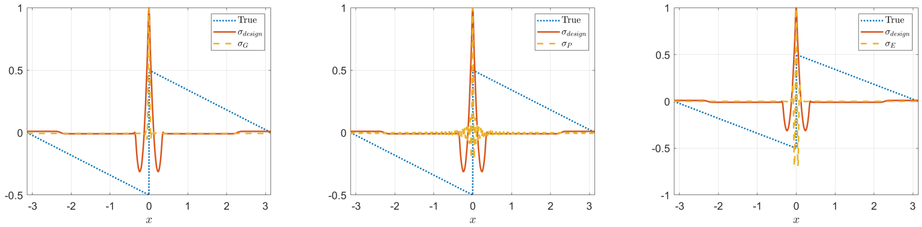

Figure 8: Jump function for the ramp function using designed concentration factors compared with (left) σ_G, (middle) σ_P, and (right) σ_E.

We see that the amplitude of the jump is correctly predicted only when using polynomial concentration factors. This worsens in the noisy case - when setting SNR = 20, we retrieve the results as seen in fig. 9.

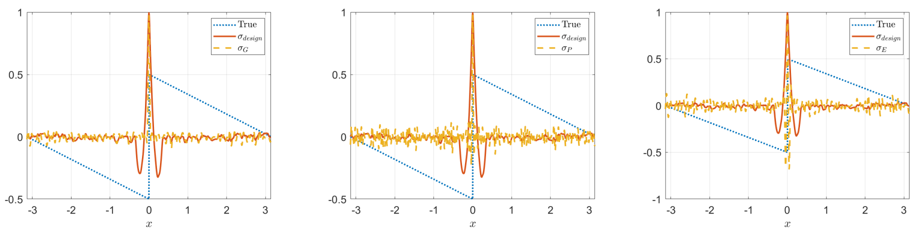

Figure 9: Jump function for the ramp function using designed concentration factors compared with (left) σ_G, (middle) σ_P, and (right) σ_E with SNR = 20.

Similarly, when looking at the noiseless case with missing bands from $-64 \leq k \leq -32 \cup 32 \leq k \leq 64$, we retreive fig. 10.

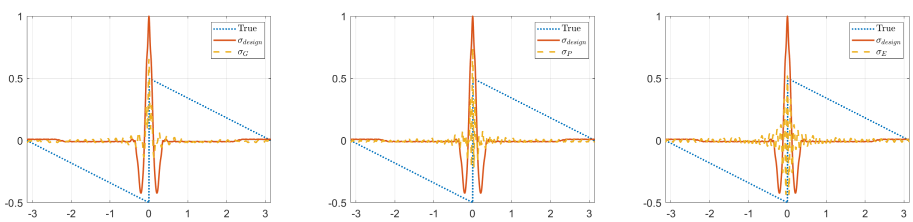

Figure 10: Jump function for the ramp function using designed concentration factors compared with (left) σ_G, (middle) σ_P, and (right) σ_E with missing bands from $-64 \leq k \leq -32 \cup 32 \leq k \leq 64$.

4.1. Box Function. In real-world problems, the underlying signal would be unknown. We would thus design concentration factors for an estimated underlying function that may not be correct. In order to test the effectiveness of the concentration factor design for estimating other, unknown function, we use the simple box function as a test function for the concentration factors designed for the ramp function.

The box function is defined as:

$$f_{box}(x) = \begin{cases} 1 & -1 \leq x \leq 1 \\ 0 & else \end{cases} \tag{4.1}$$

We first do a reconstruction of the jump function in the noiseless case with missing bands $-64 \leq k \leq -32 \cup 32 \leq k \leq 64$. We retrieve this in fig. 11:

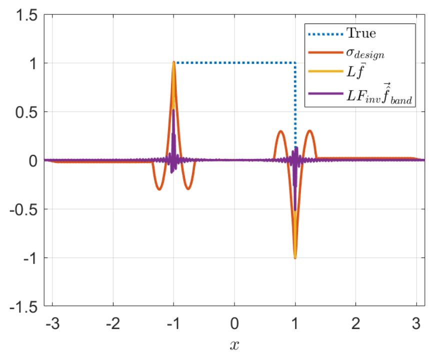

Figure 11: Jump function of box function with missing bands $-256 \leq k \leq -128 \cup 128 \leq k \leq 256$ but no noise.

We see that the jump function is properly recovered, with both jump locations with the proper amplitudes of 1 when $x = -1$ and -1 when $x = 1$. Furthermore, when adding various levels of noise with SNR $= 10$, 20, and 100 (essentially no noise) in fig. 12, we once again see that this does not affect the recovery of jump locations and amplitude.

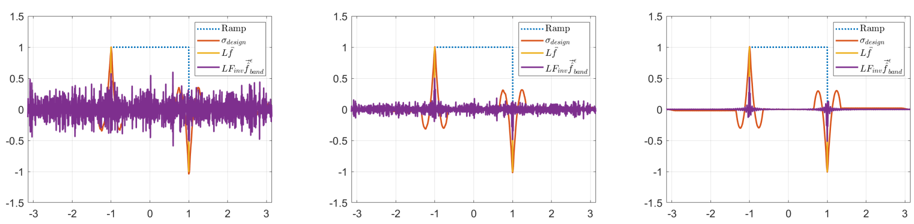

Figure 12: Jump function for the box function using the new design of concentration factors where SNR $=$ (left) 10, (middle) 20, and (right) 100, and there are missing bands of $-256 \leq k \leq -128 \cup 128 \leq k \leq 256$.

4.2. Square Wave Function. We can extend the box function to the square wave function.

We first do a reconstruction of the jump function in the noiseless case with no missing bands and compare to the use of $LF_{inv}\vec{\tilde{f}}$ as an edge recovery technique. We also test the case where we have missing bands of $-256 \leq k \leq -128 \cup 128 \leq k \leq 256$ and SNR $= 20$. These results are displayed in fig. 13:

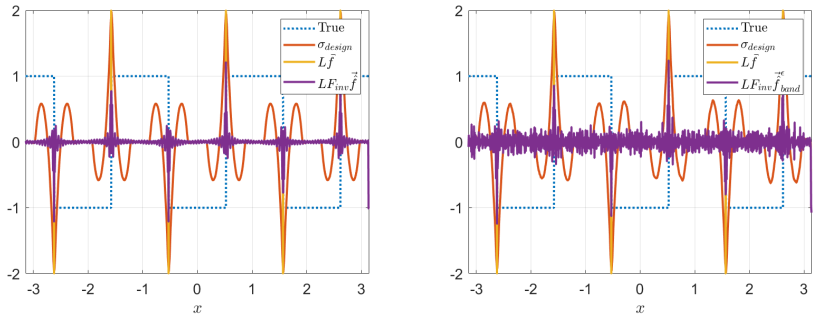

Figure 13: Jump function of square wave function with (left) no missing bands and no noise, and (right) missing bands of $-256 \le k \le -128 \cup 128 \le k \le 256$ with SNR $= 20$.

Even with noise and missing bands, the jump function reconstruction using our new design of concentration factors recovers the edge locations and amplitude accurately. However, using $LF_{inv}\vec{\hat{f}}$ and $LF_{inv}\vec{\hat{f}}^{\epsilon}_{band}$ do not provide the correct amplitudes, and the edge recovery is much more sensitive to noise as indicated by the oscillatory nature seen in the right graph of fig. 13.

We can also compare the use of our new design of concentration factors to that of the existing trigonometric, polynomial, and Gaussian concentration factors. We see in fig. 14 that for a square wave function missing bands, the amplitude of the jumps are not correctly predicted when using any of the three previous concentration factors. Here we have missing bands from $-64 \le k \le -32 \cup 32 \le k \le 64$.

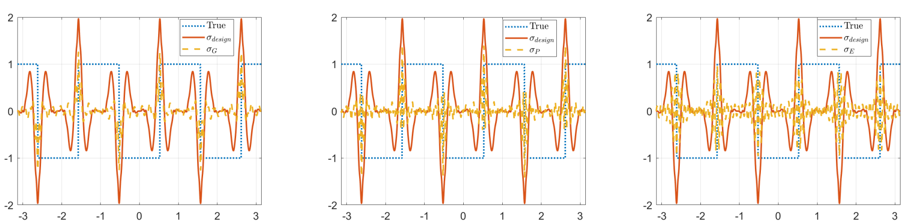

Figure 14: Jump function for the square wave function using designed concentration factors compared with (left) σ_G, (middle) σ_P, and (right) σ_E concentration factors. We have missing bands from $-64 \le k \le -32 \cup 32 \le k \le 64$.

Similarly, when looking at the noisy case with SNR $= 20$ and missing bands from $-64 \le k \le -32 \cup 32 \le k \le 64$, we retreive fig. 15 and notice that the amplitudes are once again not accurately recovered when using trigonometric, polynomial, or Gaussian concentration factors.

4.3. Multi-Feature Function. We also would like to test our recovery on functions that have multiple, different features.

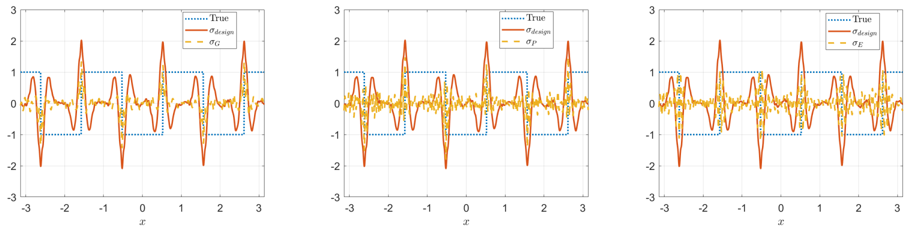

Figure 15: Jump function for the square wave function using designed concentration factors compared with (left) σ_G, (middle) σ_P, and (right) σ_E concentration factors. We have missing bands from $-64 \le k \le -32 \cup 32 \le k \le 64$ and SNR $= 20$.

$$f_{\text{multi-feature}} = \begin{cases} \frac{3}{2}, & -\frac{3\pi}{4} \le x < -\frac{\pi}{2} \\ \frac{7}{4} - \frac{x}{2} + \sin\left(x - \frac{1}{4}\right), & -\frac{\pi}{4} \le x < \frac{\pi}{8} \\ \frac{11}{4}x - 5, & \frac{3\pi}{8} \le x < \frac{3\pi}{4} \\ 0, & \text{otherwise} \end{cases}$$

Figure 16 shows the reconstruction of the jump function in the noiseless case with no missing bands, as well as the case with missing bands $-256 \le k \le -128 \cup 128 \le k \le 256$ and SNR $= 20$.

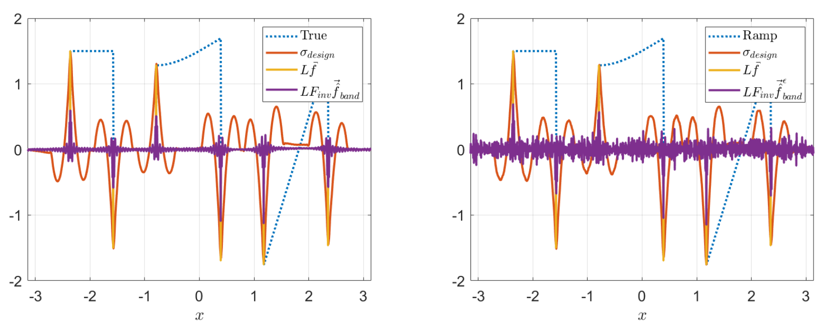

Figure 16: Jump function of multi-feature function with (left) no missing bands and no noise, and (right) missing bands $-256 \le k \le -128 \cup 128 \le k \le 256$ with SNR $=$ 20.

Even with noise and missing bands, the jump function reconstruction using our new design of concentration factors recovers the edge locations and amplitude accurately. We can see this in comparison to the trigonometric, polynomial, and Gaussian concentration factors.

We see in fig. 17 that for more complicated functions with multiple features and missing bands, the amplitude of the jumps are not correctly predicted when using any of the three previous concentration factors. Here we have missing bands from $-256 \le k \le -128 \cup 128 \le k \le 256$.

Similarly, when looking at the noisy case with SNR $= 20$ and missing bands from $-256 \le k \le -128 \cup 128 \le k \le 256$, we retreive fig. 18 and notice that the amplitudes

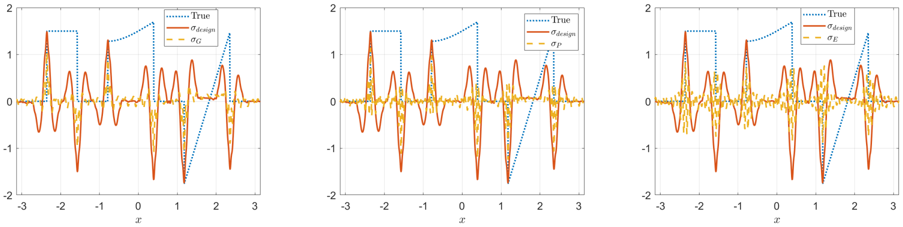

Figure 17: Jump function for the multi-feature function using designed concentration factors compared with (left) σ_G, (middle) σ_P, and (right) σ_E. We have missing bands from $-256 \leq k \leq -128 \cup 128 \leq k \leq 256$.

are once again not accurately recovered when using trigonometric, polynomial, or Gaussian concentration factors.

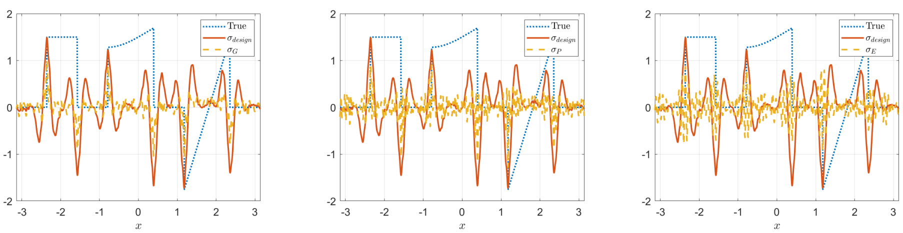

Figure 18: Jump function for the multi-feature function using designed concentration factors compared with (left) σ_G, (middle) σ_P, and (right) σ_E and SNR $= 20$.

4.4. Robustness. In order to test the robustness of our method of concentration factor design, we complete the reconstructions with 3 varying levels of N to vary the number of Fourier measurements used. We compare our jump recovery with that of using first order finite differencing in fig. 19.

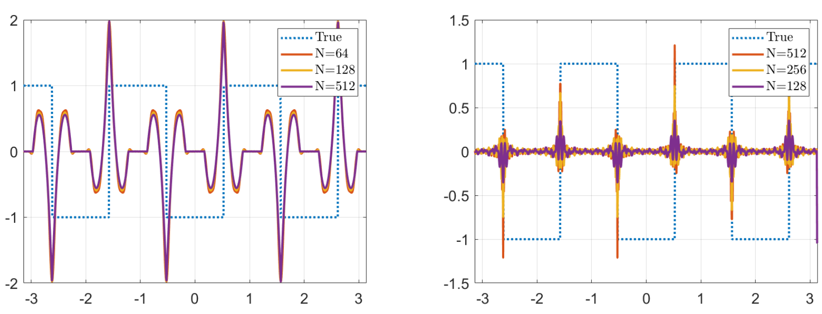

Figure 19: Jump function of a square wave function using (left) the new design of concentration factors and (right) first order finite differencing $L_1\vec{f}$ with 3 different numbers of Fourier measurements N. We have no noise and no missing bands.

We also investigate the accuracy of our jump recovery when using 3 different levels of missing band data. With $N = 512$ and 1025 Fourier coefficients, we test the effects of using no missing bands, missing bands of $-256 \leq k \leq -128 \cup 128 \leq k \leq 256$, and $-256 \leq k \leq -192 \cup 192 \leq k \leq 256$ compared to first order finite differencing as seen in fig. 20.

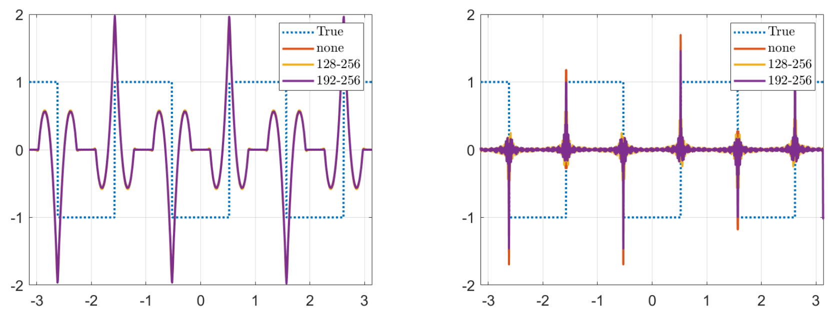

Figure 20: Jump function of a square wave function using (left) the new design of concentration factors and (right) finite differencing $L\vec{f}$ with 3 different bandwidths of missing bands: no missing bands (red), $-256 \leq k \leq -128 \cup 128 \leq k \leq 256$ (yellow), and $-256 \leq k \leq -192 \cup 192 \leq k \leq 256$ (purple).

From these plots, it can be seen that using first order finite differencing $LF_{inv}\vec{\hat{f}}_{band}$ yields inaccurate and variable jump recovery for all levels of N and missing bands. However, our concentration factor design yields robust and accurate results when varying both these factors.

4.5. Other Operators. We would also like to analyze the use of other operators L, such as higher order finite differencing matrices. Here we present a few examples of edge detection with missing bands for various estimation functions in Figure 21.

5. Concluding remarks. In conclusion, we have created a concentration factor design for a ramp function that accurately and robustly recovers the jump function of an unknown estimation function. Our method works especially well compared to existing methods such as finite differencing when considering noisy data or missing bands of data. This method can be used to help recover edge information about the underlying function to aid in further function reconstruction and recovery.

Acknowledgments. I would like to acknowledge my thesis mentor, Professor Anne Gelb, for all her support in this work. I would also like to acknowledge all the help of Professor Aditya Viswanathan of University of Michigan Dearborn. I would like to give the biggest thanks to my parents for their lifetime of support. And finally, I would like to acknowledge all who have shaped my Dartmouthe experience.

REFERENCES

[1] A. Gelb and E. Tadmor, *Detection of edges in spectral data*, Applied and Computational Harmonic Analysis, 7 (1999), pp. 101–135.

[2] J. S. Hesthaven, S. Gottlieb, and D. Gottlieb, *Spectral Methods for Time-Dependent Problems*, Cambridge Monographs on Applied and Computational Mathematics, Cambridge University Press, Cambridge, 2007.

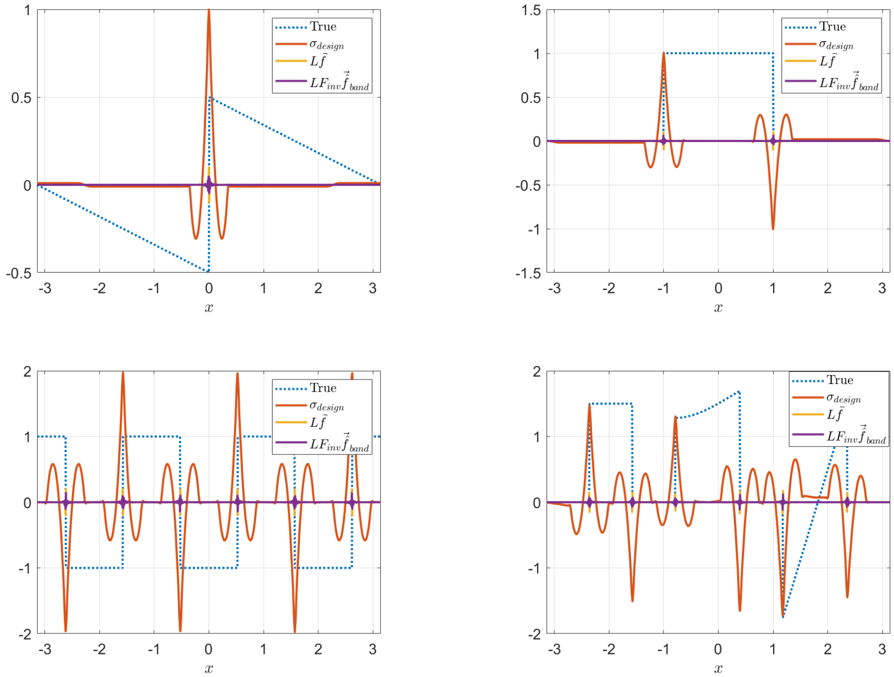

Figure 21: Plot of edge recovery using $L = L_2$, or the second order finite differencing matrix in our concentration factor design for: (upper left) ramp, (upper right) box, (lower left) square wave, and (lower right) multi-feature function. We use 1025 Fourier coefficients and missing bands of $-256 \le k \le -128 \cup 128 \le k \le 256$.

[3] A. Viswanathan, A. Gelb, and D. Cochran, *Iterative design of concentration factors for jump detection*, Journal of Scientific Computing, 51 (2012), pp. 631–649.